

See discussions, stats, and author profiles for this publication at: <https://www.researchgate.net/publication/231700749>

Simulation of End-Coupling Reactions at a Polymer–Polymer Interface: The Mechanism of Interfacial Roughness Development

ARTICLE in MACROMOLECULES · JANUARY 2011

Impact Factor: 5.8 · DOI: 10.1021/ma101285m

CITATIONS

14

READS

1,109

2 AUTHORS:



Anatoly V Berezkin

Technische Universität München

30 PUBLICATIONS 173 CITATIONS

[SEE PROFILE](#)



Yaroslav V Kudryavtsev

Russian Academy of Sciences

62 PUBLICATIONS 354 CITATIONS

[SEE PROFILE](#)

Simulation of End-Coupling Reactions at a Polymer–Polymer Interface: The Mechanism of Interfacial Roughness Development

Anatoly V. Berezkin*

Max-Planck Institut für Eisenforschung GmbH, Max-Planck Strasse 1, 40237 Düsseldorf, Germany

Yaroslav V. Kudryavtsev*

A.V. Topchiev Institute of Petrochemical Synthesis, Russian Academy of Sciences, Leninsky prosp. 29, 119991 Moscow, Russia

Received June 9, 2010; Revised Manuscript Received November 22, 2010

ABSTRACT: End-coupling between immiscible melts of two monofunctionalized polymers of a same length was modeled by dissipative particle dynamics starting from a flat interface and up to the formation of a mature lamellar microstructure. Influence of the reaction rate, chain length, and incompatibility of components on the kinetics of copolymer formation and morphology development was investigated. Regimes of linear and logarithmic growth of the conversion with time were observed before the flat interface became unstable. The conditions and mechanism of interfacial roughness development were studied in detail. It was demonstrated that overcrowding the interface with the copolymer product causing its phase separation plays the main role in spontaneous interface distortion. The instability leads to autocatalytic interface growth with exponential kinetics, when each new portion of the product creates more area for further reactions. It was followed by a slower terminal regime including formation and ripening of the lamellar microstructure. The late stage kinetics of end-coupling was strongly influenced by depletion of reactants and formation of ordered product layers. At certain conditions, it became asymptotically diffusion controlled in agreement with published experimental data.

Introduction

Design of commercial polymer composites is based on combining different species to tailor material properties.¹ However, a straightforward melt blending is often ineffective due to the tendency to phase separation in most of polymer couples. Usually it results in a small area of polymer–polymer interface and hence weak adhesion between blend components. Adding copolymers that serve as surfactants and promote adhesion by increasing contact area, forming entanglements, and introducing chemical bonds between immiscible domains can solve the incompatibility problem.

Though premade graft, block, and random copolymers are widely used, the most promising strategy is related to the so-called reactive compatibilization,^{1–5} which implies copolymer formation *in situ*. Its main advantage is that copolymers appear at the interface just where they are needed to improve thermodynamic and mechanical properties of a composite.⁶

Understanding the fundamentals of reactive polymer blending requires various contributions to be separated, which is possible only for relatively simple systems. One of the most popular models is a flat interface between melts of incompatible homopolymers A and B, end units of which are functionalized with complementary reactive groups. An end-coupling reaction produces a block copolymer AB, which modifies the interfacial tension, adhesion, etc. and in turn influences the reaction rate. Under quiescent conditions, diffusion and reaction are the only factors governing evolution of a bilayer system. Their interplay was investigated in theory,^{7–11} by simulations,^{12–16} and experimentally.^{5,17–22}

At the very beginning, the interfacial coverage n (the number of copolymer chains per unit interface area) grows linearly with time t . If the local reactivity Q of contacting end groups is much less than the inverse relaxation time for a monomer unit, which is realized in most of the experiments, then theories predict that a linear regime $n \sim t$ is followed by a diffusion controlled (DC) regime $n \sim t^{1/2}$. However, the characteristic time separating the regimes is very large being proportional to Q^{-2} so that the DC regime could be outside experimental time scales.¹⁰ Indeed, the only evidence of a “depletion hole”¹⁹ is related to the low-temperature reaction between PS–COCl and PMMA–NH₂ in supercritical CO₂, whereas melt studies with various functional groups suitable for chain coupling^{23,24} demonstrate mean field kinetics without any DC regimes.

At the same time, diffusion controlled kinetics is well reproduced in molecular dynamics,¹² Monte Carlo^{13–15} and hybrid model¹⁶ simulations, while the linear regime is distorted or not observed at all. This can be explained by unrealistically high reaction rates used in all simulations of end-coupling performed so far. In fact, it was assumed^{12–16} that each contact between reactive chain ends led to the formation of a covalent bond with probability one.

Another important factor influencing the reaction kinetics is saturation of the interface with the copolymer product. At a critical coverage $n_{cr} = 1/(3N^{1/2}b^2)$ (b is a segment size, N is a chain length assumed to be equal for both polymers) blocks start to feel one another and therefore begin to stretch. Copolymer chains gradually form a brush, which creates a potential barrier for unreacted homopolymers approaching the interface. Asymptotically, a new kinetic regime is established.⁹

$$n \sim n_{cr} \sqrt{\ln((N^{1/2}t)/(\tau_1 \ln N))} \sim (\ln t)^{1/2}$$

*Corresponding authors. E-mail: (A.V.B.) berezkin.anatoly@rambler.ru; (Y.V.K.) yar@ips.ac.ru.

where τ_1 is the terminal chain relaxation time. At weak reactivity and equal reactant concentrations, the copolymer begins retarding kinetics before the DC regime is set so that the linear regime is directly followed by the logarithmic one.

While theories are focused on the early stages of end-coupling, experiments demonstrate^{18,20,25,26} that a slowdown in the kinetics caused by interface saturation can be spontaneously superseded by acceleration, which is accompanied by abrupt roughening and emulsification of the interface. Under simple shear flow, a fine microstructure can be easily formed in the reacting system at a shear rate that is not enough to increase interface area by itself.²⁷ The similar scenario is observed in melts where coupling reactions produce graft copolymers.^{28,29}

It was shown that interface roughening does not occur and the kinetic curve levels off if reacting homopolymers are rather long ($\chi N = 10$) and therefore separated by a very narrow interface¹⁸ or if their degree of functionalization is low (< 30 wt %).²⁶ However, those particular observations do not specify sufficient conditions for interfacial roughness development and its mechanism. An attempt to explain a steep increase in roughness in the reacting blend of dPS–NH₂ and P2VP–anhydride by the vanishing interfacial tension²⁰ was later challenged by the finding that coupling between those polymers is a reversible reaction, which influences a block copolymer amount at the interface.²¹

Previous computer simulations of end-coupling also captured the possibility of accelerating the reaction kinetics at late stages.^{12,16} It was found that the flat interface became unstable after the interfacial tension had vanished, whereas subsequent growth of the interface width obeyed a diffusion law ($\sim t^{1/2}$) indicating about possible effect of thermal fluctuations. However, those studies were severely restricted in spatial and time scales by limitations in computational resources. The routine molecular dynamics simulation¹² only enabled detection of the interfacial instability. Investigating subsequent growth of fluctuations and transformation of the bilayer system into a lamellar structure¹⁶ involved a number of simplifications: initial homopolymers were modeled by hard spherical particles while block copolymers by rigid dumbbells, the coupling rate was unrealistically high, the interfacial tension was approximated by the gradient energy density, hydrodynamic effects were neglected.

In this work, we use computer simulations to reexamine evolution of an incompatible polymer melt undergoing end-coupling reactions. The study is focused on understanding reasons and kinetics of interface roughening using more realistic probabilistic reaction kinetics. We model highly concentrated systems, where every chain carries a reactive end group. This promotes formation of an interfacial block copolymer layer in a mean field (reaction controlled) kinetic regime in agreement with most of the experiments. The dissipative particle dynamics method, which is used for simulations, provides high speed of relaxation and accounts for hydrodynamic effects. As a result, time scales are attained that are 2 orders of magnitude as large as the interface saturation time t_s . This enables us to study the development of interface roughening in detail. It is found that after the flat interface becomes unstable, the reaction is characterized by exponential kinetics. Subsequent formation and ripening of lamellas are considerably influenced by diffusion of reactants.

Simulation Technique and Model

We use a coarse-grained molecular dynamics method referred to as dissipative particle dynamics (DPD). This simulation technique was proposed by Hoogerbrugge and Koelman^{30,31} and developed by Espanol, Groot, and Warren.^{32,33} Its applicability to polymer systems was substantiated by mapping DPD onto the lattice Flory–Huggins theory.³³

Consider an ensemble of interacting particles governed by Newton's equations of motion:

$$\frac{d\mathbf{r}_i}{dt} = \mathbf{v}_i, \quad m_i \frac{d\mathbf{v}_i}{dt} = \mathbf{f}_i + \mathbf{f}_i^{\text{pol}} \quad (1)$$

Here \mathbf{r}_i , \mathbf{v}_i , m_i denote the radius vector, velocity, and mass of the i th particle, and \mathbf{f}_i and $\mathbf{f}_i^{\text{pol}}$ are nonpolymeric and polymeric forces acting on it. The former force, which describes interactions in the corresponding low-molecular liquid, may be written as a sum of pairwise additive contributions:

$$\mathbf{f}_i = \sum_{j \neq i} (\mathbf{F}_{ij}^C + \mathbf{F}_{ij}^D + \mathbf{F}_{ij}^R) \quad (2)$$

where the summation is performed over all other particles within a certain cutoff radius r_c . We assume that all quantities in eq 1, 2 are dimensionless and for simplicity set all m_i and r_c to unity.

A conservative force \mathbf{F}_{ij}^C describes soft core repulsion between contacting particles

$$\mathbf{F}_{ij}^C = \begin{cases} a_{ij}(1 - r_{ij})\bar{\mathbf{r}}_{ij}, & r_{ij} < 1 \\ 0 & r_{ij} \geq 1 \end{cases} \quad (3)$$

where $\mathbf{r}_{ij} = \mathbf{r}_j - \mathbf{r}_i$, $\mathbf{r}_{ij} = |\mathbf{r}_{ij}|$, $\bar{\mathbf{r}}_{ij} = \mathbf{r}_{ij}/\mathbf{r}_{ij}$, and a_{ij} is a maximum repulsion between particles i and j attained at $\mathbf{r}_i = \mathbf{r}_j$.

Other constituents of \mathbf{f}_i are a dissipative force \mathbf{F}_{ij}^D (friction) and a random force \mathbf{F}_{ij}^R :

$$\begin{aligned} \mathbf{F}_{ij}^D &= -\frac{\sigma^2}{2k_B T} [\omega(r_{ij})]^2 (\mathbf{v}_{ij} \cdot \bar{\mathbf{r}}_{ij}) \bar{\mathbf{r}}_{ij}, \\ \mathbf{F}_{ij}^R &= \sigma \omega(r_{ij}) \frac{\xi}{\sqrt{\delta t}} \bar{\mathbf{r}}_{ij}, \quad \omega(r) = \begin{cases} 1 - r, & r \leq 1 \\ 0, & r > 1 \end{cases} \end{aligned} \quad (4)$$

where σ is a noise amplitude, k_B is the Boltzmann constant, T is temperature, $\mathbf{v}_{ij} = \mathbf{v}_i - \mathbf{v}_j$, ξ is a normally distributed random variable with zero mean and unit variance chosen independently for each pair of particles, and δt is a time step. We take that $k_B T = 1$ and define a dimensionless time unit as

$$\tau = r_c \sqrt{\frac{m}{k_B T}} = 1 \quad (5)$$

Chain connectivity of particles is introduced using the standard bead–spring model so that $\mathbf{f}_i^{\text{pol}}$ is a bond elasticity force

$$\mathbf{f}_i^{\text{pol}} = \sum_j K_{ij} \mathbf{r}_{ij} \quad (6)$$

where K_{ij} is a spring constant (we take $K_{ij} = 4$ for bonded particles and zero for others).

Following Groot and Warren³³ we choose $\sigma = 3$, the reduced particle density $\rho_0 = 3$, and $a_{ii} = 25$. In that case, a_{ij} is related to the interaction parameter χ of the Flory–Huggins theory as

$$a_{ij} = \chi/0.306 + 25, \quad i \neq j \quad (7)$$

The Groot–Warren thermostat defined by eq 4, where the random and dissipative forces serve as a heat source and sink, respectively, preserves momentum for each pair of interacting particles and therefore enables one to account for hydrodynamic effects on microphase separation in block copolymers,^{34,35} which are inaccessible by the Monte Carlo method and conventional molecular dynamics.

Simulations were performed with DPDChem freeware package.³⁶ The equations of motion 1 were solved using the so-called DPD–VV integration scheme,³⁷ which is a modified version of the velocity–Verlet algorithm (MD–VV), fast enough and more accurate than the latter. The time step $\delta t = 0.04$ was taken,

which allows to accurately model compatibilization during relatively long time intervals. Since some artifacts stemming from the choice of an integration scheme, time step, and relative intensity of dissipative and random forces in the DPD method were previously reported,³⁸ a part of our simulations was carried out at the smaller time step $\delta t = 0.02$ and almost the same kinetics was observed.

A simulation box initially contained two layers of incompatible macromonomers A and B of equal polymerization degree ($N_A = N_B = N$) taken in equal amounts and separated by a flat interface parallel to the xy plane. Periodic boundary conditions along all axes were imposed. Alternatively, impenetrable walls made of particles similar to the particles of an adjacent melt were used in the z direction. In both cases the same reaction kinetics was observed provided the difference in the interfacial area was taken into account.

Simulations were carried out in boxes of different shapes containing up to 10^5 particles at the average number density $\rho_0 = 3$. At short times ($t = 10^{-1} \div 10^3$) the best statistics were obtained for a slab of sizes $l_x \times l_y \times l_z = 50 \times 50 \times 20$ (in r_c units) with impenetrable walls perpendicular to the z axis. This can be explained by a maximum surface-to-volume ratio and number of elementary reactions per unit time attained in that box. In the range $t = 10^2 \div 10^4$ the most effective was a box of sizes $l_x \times l_y \times l_z = 25 \times 25 \times 50$ with periodic boundary conditions in all directions. At $t = 10^3 \div 10^5$, a rod-like box of sizes $l_x \times l_y \times l_z = 15 \times 15 \times 80$ and impenetrable walls in the z direction was chosen because it enabled studying the diffusion of reactants through a thick layer of the copolymer product. The last box contained 5.4×10^4 particles only and such reduction made it possible to expand the time interval for studying late stages of the process. Curves presented in the next Section were plotted using the data for a box providing the best statistics for a given time interval.

Simulations were performed for $N = 2, 5$, and 10 at the fixed repulsion parameter $a_{AB} = 50$ and for $a_{AB} = 25, 30, 35, 40, 45, 50, 60$, and 80 at the fixed macromonomer length $N = 5$. Four runs per each system were carried out starting from random initial configurations. Deviations in the kinetics for different runs never exceeded 7% at the initial stage (at a flat interface) and 3% at the late stage (after interface roughening).

It is easy to find that when N is varied, the product $\chi(N_A + N_B)$ takes the values of 30.6, 76.5, and 153.0, whereas increasing a_{AB} from 30 to 80 results in a wider range $\chi(N_A + N_B) = 15.3 \div 168.3$ ($a_{AB} = 25$ corresponds to an athermal and therefore compatible blend with $\chi = 0$). The lower boundary of that range corresponds to the outset of the strong segregation regime in a pure AB copolymer melt,³⁹ when block conformations are close to Gaussian, whereas the upper boundary lies within the superstrong segregation regime,⁴⁰ when blocks are highly stretched. In any case, blocks of the copolymer product are rather incompatible and therefore tending to form a brush at the A/B interface. According to the strong segregation theory,³⁹ the phase behavior of a polymer system is determined by the product χN and DPD correctly reproduces this scaling.³⁴ Therefore, properties of low $N - \text{high } \chi$ systems studied by simulations can be mapped onto those of high $N - \text{low } \chi$ blends usually investigated in laboratory experiments.

Chemical reactions were modeled using the probabilistic approach based on the following principles.

1. Two active centers can react (form a new bond) at a short distance only, which is called the reaction radius r_R .
2. Each pair of contacting active particles has to be considered for the possible reaction in a random order.
3. Reaction in every pair proceeds with a certain pre-defined probability p_R .

4. If the average number of pairs simultaneously formed by an active center equals η , then p_R value should obey the rule $\eta p_R < 1$ to prevent underestimating the reaction rate.

Similar approaches were implemented in MD,^{41,42} DPD,⁴³ and Monte Carlo⁴⁴ simulations of polymerization.

In this work, the probability of end-coupling per unit time was chosen to be $p_R = 0.0025, 0.025$, or 0.25 for each pair of reactive particles situated within the distance $r_R = r_c = 1$. The reaction procedure was carried out every tenth integration step. First of all, pairs of reactive particles separated by distances $r \leq 1$ were detected. Then, for each pair a random number λ ranging from 0 to 1 was generated and compared to p_R . At $\lambda < p_R$, the reaction took place and a new bond was irreversibly formed. If several complementary particles were closer than r_R from a given reactive particle, then the reaction was attempted with each of those particles in order of distances to them.

According to the generalized Flory principle, at a fixed reaction probability, the effective reaction rate should be the same for macromonomers of different lengths. However, our simulations demonstrated that it slowly decreases with N . It can be explained by displacement of reactive particles B from the surrounding of a given reactive particle A (and vice versa) by its unreactive macromonomer tail. The longer the tail is the lower is the local concentration of B particles. This effect can be quantified in terms of the parameter

$$\gamma = \frac{4\pi}{V_R} \int_0^{r_R} r^2 g(r) dr < 1 \quad (8)$$

where $g(r)$ is the AB pair correlation function and integration is performed over the reaction radius r_R , $V_R = 4\pi r_R^3/3$. By definition, γ is a ratio of the concentration of reactive particles B within the reaction radius of particle A and their mean bulk concentration. Considering a homogeneous end-coupling of two miscible macromonomers, we found $\gamma = 0.9023, 0.8778$, and 0.8751 for $N = 2, 5$, and 10 , respectively, i.e., the apparent reactivity slowly decreases with the tail size resulting in the 3% difference between the longest and shortest chains. A similar effect is expected for the reaction at a polymer/polymer interface. In the present simulation, it is neglected but should be taken into account when reactions in highly polydisperse or branched systems, such as radical polymerization or network formation, are modeled.

The relation between DPD time and real time can be roughly found as follows. Consider a homogeneous coupling between reactants A and B of densities ρ_A and ρ_B , which obeys the second-order kinetics:

$$\frac{\partial \rho_A}{\partial t} = -k \rho_A \rho_B \quad (9)$$

The characteristic time of this reaction is $\tau_h = 1/(k\rho_B^0)$, where ρ_B^0 is the initial value of ρ_B . For our DPD model, $k = \gamma V_R p_R \approx 4\pi p_R/3$, $\rho_B^0 = \rho_0/N_B = 3/N$ so that $\tau_h \approx N/(4\pi p_R)$ is varied from 0.6 for $N = 2$ and $p_R = 0.25$ to 3×10^2 for $N = 10$ and $p_R = 0.0025$. The corresponding experimental value of τ_h can also range in wide limits for reacting groups of different chemical nature. For example, $k \approx 10^2 \text{ kg}/(\text{mol} \cdot \text{min})$ at 180 °C was reported⁴⁵ for aliphatic amine and anhydride attached to the ends of PMMA chains. The reaction rate was limited by the amine initial concentration of $\rho_B^0 = 3.5 \text{ mmol}/\text{kg}$, which yields $\tau_h \approx 1.7 \times 10^2 \text{ s}$. Therefore, the unit time for our slowest DPD simulation is equivalent to 0.57 s in the mentioned experiment.

The same reacting groups were used for studying an interfacial reaction between PS (18 kg/mol) and PMMA (23 kg/mol) layers at 175 °C.²⁶ After 10 min, which corresponds to ca. 10^3 units of

DPD time, a significant interface roughening was detected. In order to study late stages of the reaction, longer runs are needed so the simulations in this work were carried out up to 10^5 DPD time units.

As there are two dynamic processes in the modeled system, that is, chemical reaction and diffusion, it is instructive to compare their rates. Consider an initial bilayer melt of end-functionalized macromonomers A and B of densities $\rho_A^0 = \rho_B^0 = \rho_0/N$. The local reaction time for two contacting particles A and B is $\tau_R \approx 1/p_R$. Coupling takes place within an interfacial layer, the width h of which depends on the degree of macromonomer incompatibility. The interfacial area per reacting pair is $s = N/(2hp_0)$, where it is taken that the end-group concentration at the interface is twice as high as in the bulk.⁴⁶ The time necessary for a particle to explore this area by diffusion equals $s/(4D) = N/(8Dhp_0)$ and, since both types of reactive particles are mobile, the local diffusion time reads $\tau_d = N/(16Dhp_0)$, where D is the macromonomer diffusivity. The ratio $\tau_d/\tau_R = p_R N/(16Dhp_0)$ determines, whether the reaction is kinetically ($\tau_d/\tau_R \ll 1$) or diffusion ($\tau_d/\tau_R \gg 1$) controlled. Taking that $h \approx 1$, $\rho_0 = 3$, and $D = 0.16273$, 0.063909 , and 0.03151 for $N = 2, 5$, and 10 , respectively,⁴⁷ we estimate that for our model systems $6.4 \times 10^{-4} \leq \tau_d/\tau_R \leq 1.7$, i.e., a diffusion control is not expected. The lowest value of τ_d/τ_R ratio is consistent with the experimental data,⁴⁸ whereas in the previous simulations,^{12–16} where particles reacted immediately after contact ($p_R = 1$), the role of diffusion was markedly overestimated.

It is known that the viscosity of DPD liquids is very low and this problem can be alleviated by using the Lowe–Anderson thermostat⁴⁹ as an alternative to eq 4. However, the above estimates allow concluding that it is hardly applicable in our case because higher viscosity would lead to decreasing the diffusion rate and hence emerging diffusion controlled regimes outlying most of the experimental observations.

Results and Discussion

Mean Field Linear Kinetics. The initial kinetics of end-coupling at a polymer/polymer interface approximately obeys the second-order mean field law^{7,8}

$$\frac{dn}{dt} \approx k_0 \rho_A^0 \rho_B^0 \quad (10)$$

where n is the copolymer coverage assuming a flat interface (the number of copolymer chains per unit area of the xy face of the simulation box), ρ_A^0 and ρ_B^0 are the initial bulk densities of reactive end groups, and k_0 is the reaction rate constant ($k_0 \sim p_R$). Since all macromonomers are of the same polymerization degree $N_A = N_B = N$ and functionalized with one reactive group, then $\rho_A^0 = \rho_B^0 = \rho_0/N$, where ρ_0 is the total particle density, which is assumed to be constant for a DPD liquid.

Neglecting the decay of reactants on a short time scale, we integrate eq 10 and get a linear dependence of n on time:

$$n = K \frac{p_R}{N^2} t, \quad K = \text{const} \quad (11)$$

Corresponding renormalization of the time scale gives a universal $n(t)$ dependence for the earliest stage of the reaction (Figure 1). Coincidence of the kinetic curves for different values of N and p_R corroborates that the chosen range of end-coupling probabilities indeed corresponds to the mean field regime.

Formation of the Copolymer Layer. As is seen from Figure 1, the linear stage is over at $tp_R/N^2 \approx 0.03$. According to the theoretical analysis by O’Shaughnessy and Vaylonis,¹⁰ the model parameters chosen for our simulation (low reactivity, complete functionalization of macromonomers, equal polymerization degree) make it possible to avoid DC kinetics

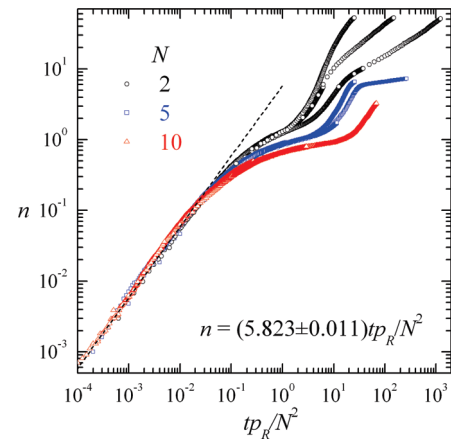


Figure 1. End-coupling kinetics: the dependence of the copolymer interfacial coverage n on scaled time. Curves are plotted for $N_A = N_B = N = 2, 5, 10$, $p_R = 0.25, 0.025, 0.0025$. The repulsion parameter $a_{AB} = 50$ in all the cases. The linear fit at the initial stage according to eq 11 is shown by the dashed line.

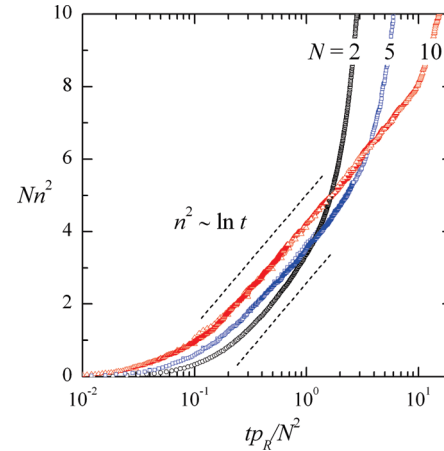


Figure 2. Saturation stage of end-coupling. Simulation curves and parameters are as in Figure 1. The slope of the logarithmic fit $n \sim (\ln t)^{1/2}$ is shown by dashed lines.

so that the linear regime is followed by the saturation regime when the reaction rate is slowed down due to adsorption of the copolymer product at the interface.

It is demonstrated in Figure 2 that there exists a range when the kinetic curves for $N = 5$ and 10 indeed obey the logarithmic dependence

$$n(t) \sim n_{\text{cr}} \sqrt{\ln((N^{1/2}t)/(\tau_1 \ln N))}$$

predicted by Fredrickson and Milner⁹ using the brush model for an adsorbed copolymer. The duration of the saturation regime increases with the chain length because brushes of longer chains create higher thermodynamic barrier for the reactants. This effect is clearly seen in Figure 1, where nonlinearity of the curves is revealed earlier with increasing N . Termination of the regime is steeper also for longer chains. The logarithmic dependence is almost unobservable at $N = 2$ as a brush hardly can be formed by chains consisting of four units.

As in Figure 1, the curves for different reaction probabilities are coincident in Figure 2 indicating that the kinetics stays reaction controlled at least up to the end of the saturation regime.

Notwithstanding the adsorption layer suppresses end-coupling, the reaction continues and new portions of the product are

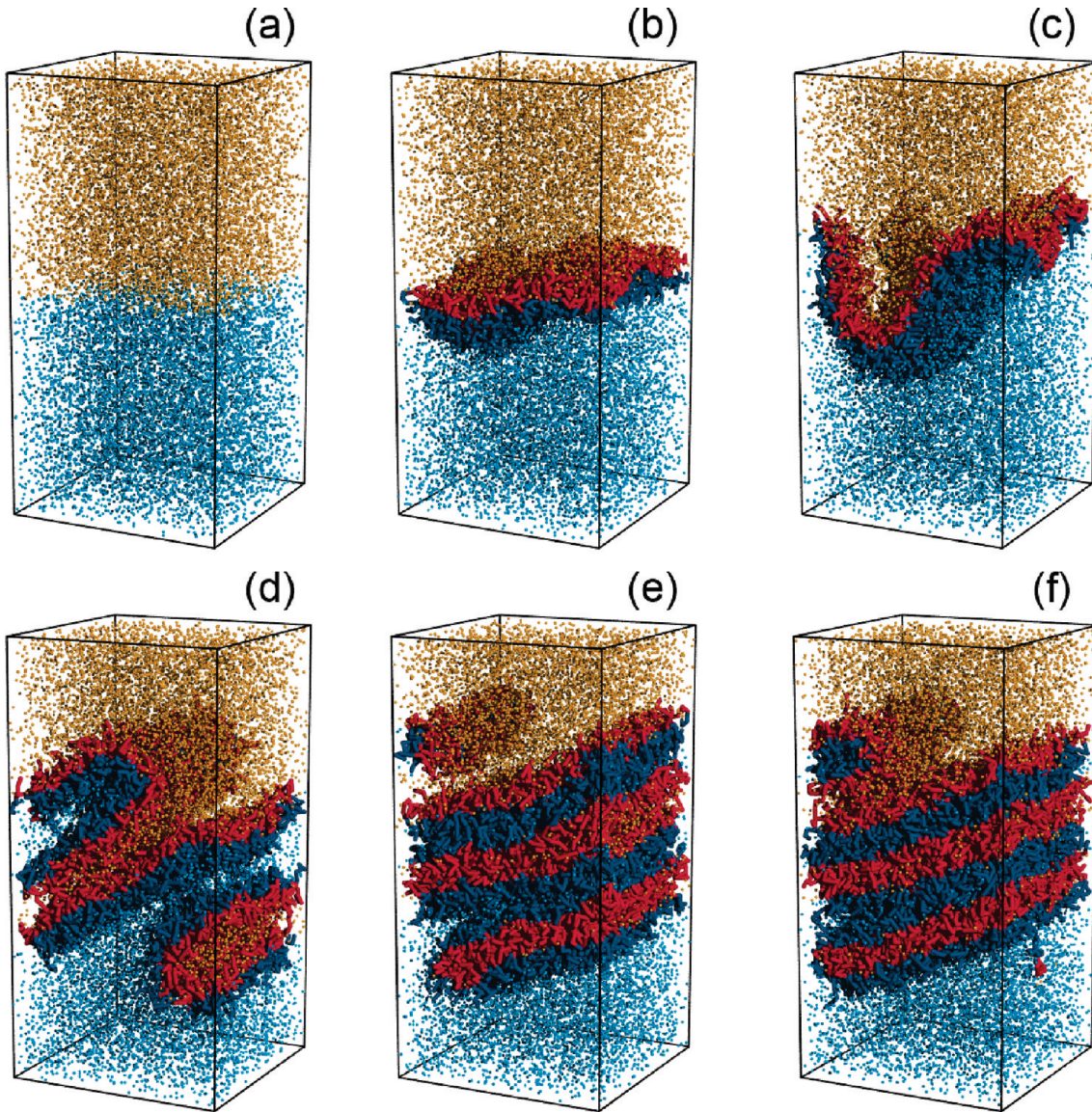


Figure 3. Snapshots of the reacting blend in the box of sizes $25 \times 25 \times 50$ with impenetrable walls. Shown are active ends of the macromonomers (A groups in orange; B ones in light blue) and copolymer chains (A particles in red; B ones in dark blue): the initial system (a), saturated layer at $t = 400$ (b), and perturbed interface at $t = 1000$ (c), forming a lamellar microstructure at $t = 2000$ (d), 3000 (e), and 4000 (f). $p_R = 0.25$, $N = 5$, and $a_{AB} = 50$.

formed at the interface. According to experimental observations^{18,20,25,26,28,29} and simulations^{12,16} this can lead to an interfacial instability. Such behavior is reproduced in our simulations as well. Each kinetic curve in Figure 1 demonstrates an inflection point at a certain time t_s , which is called a saturation time marking the end of the corresponding regime.

The main questions are why and when does the instability arise, and what governs the reaction kinetics at later stages.

Interfacial Instability in the Reacting Blend. Figure 3 clearly demonstrates a buildup of lamellar microstructure after the flat interface becomes unstable.

The emerging microstructure, which is formed by diblock copolymer chains, strikingly resembles the result of a microphase separation. Based on these observations, we put forward a hypothesis that the interface roughening can be interpreted as a response of the growing diblock copolymer layer, when its density attains a maximum value corresponding to the equilibrium density of chains in lamellas formed by a pure copolymer melt, c_∞ .

In order to calculate c_∞ , we modeled by DPD the microphase separation in a melt of pure AB copolymer having the

same characteristics as the copolymer formed by end-coupling (see Appendix A).

The interfacial copolymer coverage for a reacting bilayer system, n , which is calculated by dividing the number of copolymer molecules by the xy face area of the simulation box, S_{xy} , does not coincide with the interfacial density because even the initial interface between homopolymers is not perfectly flat. Its area S_0 found by applying the triangulation procedure⁵⁰ (see Appendix B) and dividing the resulting area by S_{xy} is given in Table 1 for the fixed block length $N = 5$ and repulsion parameter a_{AB} varying in the range $30 \div 80$. It is seen that S_0 naturally decreases with growing incompatibility of the blend components. At $a_{AB} = 25$ the blend is compatible and no A/B interface exists.

Thus, the true copolymer density at the unperturbed interface is n/S_0 and it should be compared to the density of pure copolymer in lamellas c_∞ from Table A2. We calculated $n^* = c_\infty S_0$ and marked these values on the kinetic curves $n(t)$ in Figure 4.

It is seen that in all cases they are indeed close to the inflection points so that c_∞ well approximates the maximum

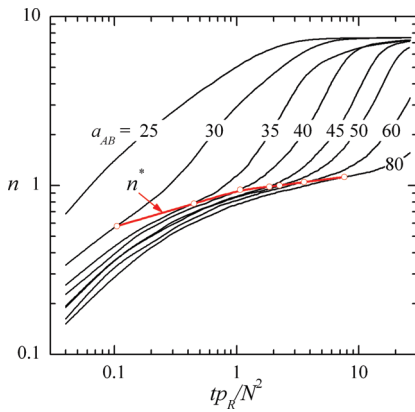


Figure 4. Copolymer interfacial coverage n vs scaled time for different values of the repulsion parameter a_{AB} , $p_R = 0.025$, $N = 5$. The red curve is drawn through the points that correspond to the interfacial coverage for a pure copolymer melt forming lamellas under the same conditions.

Table 1. Interfacial Area in the Melt of Incompatible Homopolymers A and B ($N_A = N_B = 5$)

a_{AB}	30	35	40	45	50	60	80
S_0	1.6169	1.2819	1.2495	1.2219	1.1814	1.1661	1.1331

copolymer interfacial density reached in the saturation regime. In other words, $n^* \approx n(t_s)$. Growth of n^* with a_{AB} can be explained by increasing the equilibrium domain width due to the stretching of copolymer chains, however, the dependence appears to be rather weak, in accordance with the strong segregation theory prediction $d \sim \chi^{1/6}$.³⁹ The characteristic saturation time t_s is much more sensitive to the blend incompatibility. As is seen from Figure 4, retardation of the kinetics is mostly pronounced at the end of the saturation regime so that forming a slightly denser layer (compare the curves for $a_{AB} = 30$ and 80) requires up to 2 orders of magnitude more time.

Thus, overcrowding the interface with the reaction product may be called the main reason for a spontaneous interfacial instability. Roughening and subsequent microstructure formation should be governed by the same driving forces as microphase separation in a pure copolymer, namely, the repulsion of dissimilar blocks, excluded volume interactions of blocks of one type and their conformational entropy.

It is interesting to compare the characteristic time of a microstructure formation in the diblock copolymer melt ($t_{1/2}$ from Table A1) and the interface saturation time t_s for the reacting blend. For $N = 10$ the saturated copolymer layer is formed at $t_s p_R/N^2 \approx 7$ that corresponds to a span $t_s = (2.8 \div 280) \cdot 10^3$ (depending on p_R), which is much larger than $t_{1/2} \approx 470$ (Table A1). At $N = 5$ we have $t_s p_R/N^2 \approx 2$, $t_s = 200 \div 20000$, $t_{1/2} \approx 380$ so that for the fastest reaction t_s and $t_{1/2}$ become comparable. For $N = 2$, $t_s p_R/N^2 \approx 1$ and $t_s = 16 \div 1600$, $t_{1/2} \approx 160$ and only at the highest reaction rate the rule $t_s \geq t_{1/2}$ is violated. Thus, for most of the modeled reacting systems, the saturated copolymer layer should be in a quasi-equilibrium state with respect to microphase separation. If the reaction were stopped, the instant spatial structure would not change. This statement was directly verified by simulations and appeared to be true.

In the previous studies,^{12,16,20} the genesis of interfacial instability during reactive compatibilization was related to a drop in the interfacial tension. This macroscopic characteristic is introduced by integrating the difference of normal and tangential components of the pressure tensor across the

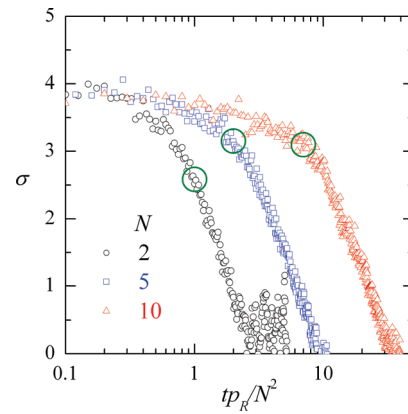


Figure 5. The dependence of the interfacial tension on scaled time for different block lengths at $a_{AB} = 50$. Large circle on each curve corresponds to the saturation time $t = t_s$, when $n = n^*$ is attained.

interface.⁵¹

$$\sigma = \int_0^z (p_n(z) - p_t(z)) dz \quad (12)$$

Unfortunately, there is no unambiguous way to compute the normal (p_n) and tangential (p_t) components of the pressure tensor for a heterogeneous mixture. If, however, there is a flat interface in the modeled system, then the Kirkwood–Buff convention⁵² may be used. The simulation box is divided into equal layers parallel to the xy plane and the local components of the pressure tensor are calculated:

$$p_n(z) = \rho_0(z) + \frac{1}{V} \left\langle \sum_{i \neq j}^{(k)} \frac{z_{ij}^2}{r_{ij}} F_{ij}^C \right\rangle, \\ p_t(z) = \rho_0(z) + \frac{1}{2V} \left\langle \sum_{i \neq j}^{(k)} \frac{x_{ij}^2 + y_{ij}^2}{r_{ij}} F_{ij}^C \right\rangle, \quad (13)$$

$$F_{ij}^C = \begin{cases} a_{ij}(1 - r_{ij}) + K_{ij}r_{ij}, & r_{ij} < r_c \\ K_{ij}r_{ij}, & r_{ij} \geq r_c \end{cases}$$

Here ρ_0 is the average particle density in a slab with coordinate z , V is the layer volume, F_{ij}^C is the conservative repulsion force acting between i and j particles separated by the distance r_{ij} . The summation runs over all pairs of particles within a given slab.

The dependence of the interfacial tension σ on simulation time is shown in Figure 5. The tension is moderately decreased during the saturation regime but it remains clearly positive at $t = t_s$ when a critical amount of the copolymer product $n = n^*$ is attained and the interfacial instability begins to develop. Therefore, in our simulations the vanishing interfacial tension is not a prerequisite for the blend emulsification. Since the interfacial energy is far from zero, thermal fluctuations are not expected to considerably contribute to the development of interfacial instability, contrary to the conclusions of ref 16.

The subsequent steeper drop in σ observed in Figure 5 is related to deformations of the interface. However, a quantitative interpretation of data for the region where the interfacial tension is close to zero is hardly possible because multiple interfaces of a forming lamellar microstructure are not necessarily oriented perpendicular to the z axis, and therefore, eq 12 becomes inapplicable. Similar methodological difficulties were mentioned earlier in the literature.¹³

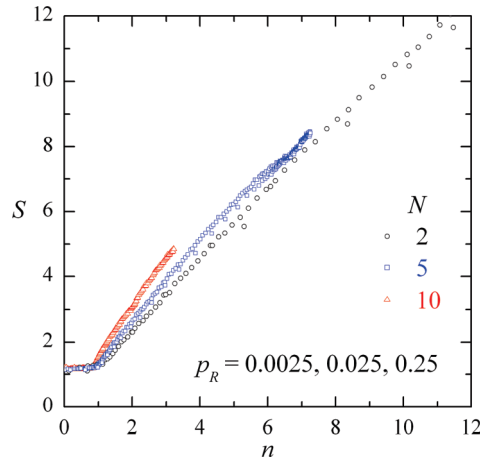


Figure 6. The total interfacial area vs the number of copolymer molecules formed by end-coupling (both divided by the xy face area of the simulation box) at $a_{AB} = 50$. The data for $p_R = 0.25, 0.025$, and 0.0025 almost coincide at a fixed N .

Our findings correlate with the results of studies on compatibilizing polymer blends with premade copolymer additives. For a blend of PS and PMMA, it was argued^{53,54} that the stability of a dispersed phase, especially under blending conditions, could be provided by a small (several wt %) amount of copolymer, which did not cause a significant reduction in the interfacial tension. Steric interactions of diblock copolymer shells covering droplet phase particles and hindering their coalescence were proposed as the main mechanism of stabilization.

Late Stage Kinetics. The interfacial density c_∞ , which is attained just before the instability manifests itself, is kept nearly constant during its development. This is demonstrated in Figure 6, where the dependence of the total interfacial area on the amount of copolymer product is plotted up to the end of simulation. As long as the single flat A/B interface is retained (for $n \leq 1$), its area does not deviate much from the initial value S_0 . However, later the interfacial area grows almost linearly with the copolymer amount so that the ratio n/S , which is nothing else but the interfacial copolymer density, remains approximately equal to $n^*/S_0 = c_\infty$. It is worth noting that c_∞ , calculated as the thermodynamically equilibrium value for a pure copolymer melt, has the same meaning for the reacting system because it is almost independent of the reaction rate p_R at a fixed block length N .

Nearly linear dependencies $S(n)$ in Figure 6 correspond to an apparent rise of the kinetic curves in Figure 1 after the inflection point ($t = t_s$). If those curves are plotted in the semilogarithmic scale of Figure 7, their linear parts are clearly visible. It means that the kinetics is exponential and the reaction proceeds in an autocatalytic regime starting at $tp_R/N^2 \approx 1$ when the copolymer interfacial coverage $n \approx 1$ so that the initial flat interface is saturated with copolymer chains.

Close correspondence between Figures 6 and 7 indicates that during the autocatalytic regime end-coupling still obeys the second-order mean field law

$$\frac{dn}{dt} = k\rho_A\rho_B \quad (14)$$

Indeed, the effective rate constant k is proportional to the instant interfacial area S , which in turn linearly increases with the copolymer amount n as it follows from Figure 6:

$$\frac{k}{k_s} \approx \frac{S}{S_0} \approx \frac{n}{n^*} \quad (15)$$

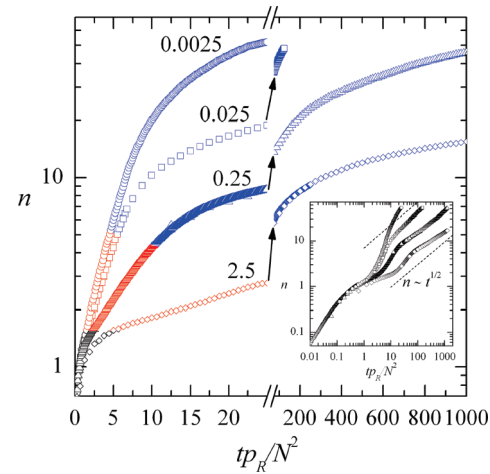


Figure 7. End-coupling kinetics at the late stage for $N_A = 2$, $a_{AB} = 50$ and different reaction probabilities p_R . Curve parts corresponding to the autocatalytic and terminal regimes are shown in red and blue, respectively. In the inset, the same curves are plotted in bilogarithmic coordinates to compare their terminal parts with the dashed lines corresponding to the pure DC kinetics ($n \sim t^{1/2}$).

Constants in the denominator of eq 15 correspond to the instability onset at $t = t_s$, when $n = n^*$, $S = S_0$, and $k = k_s$.

If we neglect a decrease in the initial reactants ($\rho_A = \rho_B \approx \rho_0/N$), then $dn/dt \sim n$. Integrating eq 14 we obtain that the total number of copolymer molecules per unit area of the box face grows exponentially in time:

$$n = n^* \exp(k_s \rho_0(t - t_s)/(N^2 n^*)) \quad (16)$$

as is observed in Figure 7 for all modeled systems.

The duration of the autocatalytic stage decreases with increasing the reaction probability p_R (note that the abscissa coordinates in Figure 7 are proportional to the product tp_R rather than t itself). It correlates with our finding that the fastest reaction for $N = 2$ leaves microphase separation of the copolymer behind its formation ($t_s \leq t_{1/2}$). In other words, in the last case copolymer chains have not enough time to set up a quasi-equilibrium lamellar structure and this results in a lower interface area and higher copolymer density thus retarding end-coupling and deteriorating mean-field kinetics described by eq 16.

In order to emphasize this effect, we modeled the system behavior at even higher reaction rate $p_R = 2.5$, when macromonomers A and B react immediately at their first contact. In that case, the earliest linear stage is not visible at all, which agrees well with the previous simulations of end-coupling,^{12,13} and only the final stage of the saturation regime is reproduced. As is seen from Figure 7 and especially from its inset, the corresponding curve has an inflection point at $tp_R/N^2 \approx 5$ and the subsequent autocatalytic regime is rather short.

For chains of 10 ($N = 5$) and especially of 4 beads ($N = 2$) it is superseded by a terminal regime with slower kinetics, just as the linear regime at the early stage is followed by the saturation one. It could happen that for longer chains of 20 beads ($N = 10$) the slowdown in kinetics is not attained due to computing restrictions.

In the terminal regime, the density of unreacted end groups decreases and the role of diffusion unavoidably grows. If the kinetic curves for $N = 2$ are plotted in the double logarithmic coordinates, they become linear (see inset in Figure 7) though the slope is not precisely equal to $1/2$ and depends on the reaction rate. It means that a true diffusion

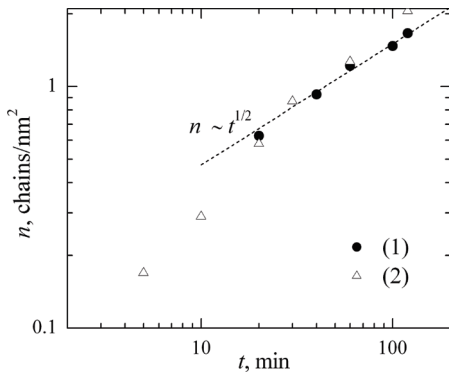


Figure 8. Coverage of an initially flat PS/PMMA interface by copolymer chains formed *in situ* according to the experimental data of ref 18 (1) and ref 26 (2). A dashed line shows the DC trend.

controlled regime is probably still not attained by simulations and some mixed type of kinetics is observed.

Yin et al.¹⁸ applied SEC-UV for monitoring an end-coupling reaction in the PS/PMMA pair. Using anthracene-labeled PS chains as a probe, the authors directly measured the dependence of the copolymer interfacial coverage n on time. In the course of the reaction, the interfacial roughness sharply increased and n attained the value of ca. 1 chain per square nm of a flat interface, which is by an order larger than the equilibrium coverage n^* extracted from measurements of the lamellar spacing in a symmetric PS-*b*-PMMA copolymer of the same molecular weight (32 kg/mol). Note that the product $\chi(N_A + N_B)$ was equal to 12, which is quite close to our DPD parametrization. In a very similar research,²⁶ where the same macromonomers with the molecular weight of 18 kg/mol at $\chi(N_A + N_B) = 12.7$ were used, it was found by AFM that the interface roughness considerably increased after 5–10 min of annealing and afterward stayed approximately constant for 2 h. The kinetic curves obtained in refs 18 and 26 are plotted in Figure 8 in double logarithmic coordinates. It is seen that at the late stage ($t > 20$ min) the diffusion controlled kinetics ($n \sim t^{1/2}$) is asymptotically established, which is consistent with the terminal regime behavior in our simulations.

It is also worth mentioning a striking likeness of the whole kinetic curve $n(t)$ obtained in our work and the time dependence of the complex viscosity measured by Kim et al.²⁸ for a reacting blend of end-functional monocarboxylated PS and poly(methyl methacrylate-*ran*-glycidyl methacrylate). There is a second-order kinetics at the initial stage of the process, then retardation, and a first-order diffusion controlled regime in between (which is not observed in our case due to the high concentration of reactants). For some time, the viscosity stays constant, which corresponds to the slow reaction in a saturated copolymer layer. Later, a fast growth in conversion accompanied by a sharp increase in the interfacial roughness measured by AFM takes place,²⁸ similarly to our autocatalytic regime. Finally, the blend viscosity stops growing and tends to a constant value thus resembling the simulated behavior in the terminal regime.

The evolution of the interfacial morphology is visualized in Figure 9, which is similar to Figure 3 but reports on simulations with the shortest macromonomers carried out in a long narrow box, i.e., under conditions mostly suitable to follow late stages of the process. It is seen that the interface is disordered in the autocatalytic regime (at $2.5 < tp_R/N^2 < 7.5$), whereas a pronounced lamellar structure arises only in the terminal regime. Ordering starts in a “long-living” central region and gradually expands over the box volume.

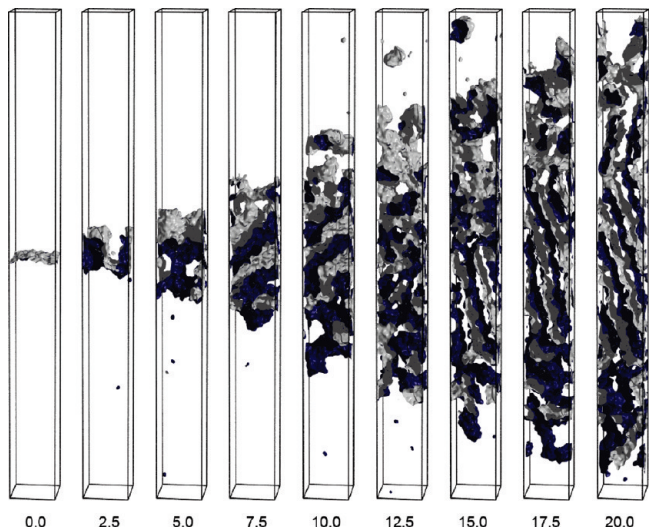


Figure 9. Interface in the reacting system ($N = 2, p_R = 0.0025, a_{AB} = 50$) at different moments of time. The values of tp_R/N^2 are shown below simulation boxes.

Very similar micrographs of partially ordered structures by TEM and AFM were obtained by Lyu et al.²⁵ who studied the reactive compatibilization in a bilayer system of PS end-capped with primary amine and PMMA end-capped with anhydride. It was demonstrated that the interfacial instability leads to a disordered morphology, which gradually transforms into local lamellar order.

Interestingly, in all our simulations lamellas are slanted like in Figure 9. Such orientation seems kinetically more stable when new copolymer chains are continuously formed. Initially, domains with all possible orientations of the interface appear but later some kind of a selection takes place. Lamellas that are parallel to the initial interface become unstable due to the lack of free space for their lateral growth. Quite the opposite, inclined lamellas can grow longer without realignment and therefore they survive in the course of the evolution in a reacting system. At the same time, a specific orientation of lamellar microdomains in our studies is related to the confined geometry of a simulation box rather than to real physical phenomena. Experiments²⁵ demonstrate that the orientation of domains is more or less arbitrary being governed by large-scale hydrodynamic fluctuations, which cannot be reproduced in a small model system.

Conclusions and Outlook

DPD modeling technique was applied for the first time to simulate *in situ* reactive compatibilization of immiscible polymer melts initially separated by a flat interface. Combining the molecular dynamics with probabilistic kinetics of an end-coupling reaction made it possible to reproduce the mean field (linear) and saturation (logarithmic) regimes at the early stage of the process, which is characterized by a low interface roughness. Such behavior is in the better agreement with experimental data than the results of preceding simulations, where too high reaction rates were used in order to observe diffusion controlled regimes, though very uncommon in laboratory experiments on macromolecular reactions.

The most attention in our work was paid to the practically interesting phenomenon of interfacial instability. Its mechanism was revealed through detailed analysis of the copolymer accumulation at different reaction rates, lengths of the initial polymers and repulsive interactions between their units. It was found that under realistic experimental conditions the interface roughening

just indicates microphase separation taking place when the interfacial copolymer density exceeds its equilibrium value. This important conclusion was supported by modeling the dynamic behavior of pure diblock copolymer melts with corresponding characteristics. It was demonstrated that the copolymer density at a newly formed interface in the reacting system is close to that in the microdomain structure of a pure copolymer melt. Thus, the interfacial instability development during reactive compatibilization is an irreversible, thermodynamically beneficial process, which however takes place only as long as the chemical reaction proceeds. As was shown, the interface roughening occurs before a substantial decrease in the interfacial tension takes place and therefore is not governed by thermal fluctuations.

It was found that after the interface distortion the reaction proceeds in an autocatalytic regime characterized by exponential kinetics, which is followed by a terminal, diffusion-controlled-like regime. It is during that experimentally observable stage the microdomain copolymer structure at first arises in the region where the initial interface was situated, then gradually expands in both directions and ripens until reactants are completely exhausted. Of course, under blending conditions the ordered regions could be also carried away by convective flows.

In this work, only lamellar microstructures were observed because of equal length and amount of modeled reactive polymers. It would be interesting to simulate reactive compatibilization in asymmetric systems, where microphase separation of the reaction product could result in different morphologies. Even more complex is the case of polydisperse melts, in which the preferential length and/or composition of a copolymer would be time dependent so that one may anticipate the formation of gradient microstructures with some characteristics depending on a distance from the initial polymer/polymer interface.

Acknowledgment. The work was supported by the Program of Fundamental Studies No. 3, Division of Chemistry and Materials Science, Russian Academy of Sciences. The authors thank Prof. P. G. Khalatur for useful discussions. They are also grateful for the opportunity to use computational cluster Chebyshev at the Moscow State University.

Appendix A. Microphase Separation in a Diblock Copolymer Melt

In this Appendix we consider the dynamics of microphase separation in a melt of pure AB diblock copolymer having the same characteristics as the copolymer formed by end-coupling. Our aim is to calculate equilibrium parameters of the microstructure and a characteristic time of its formation.

Simulations were performed in a box of sizes $30 \times 30 \times 30$ with periodic boundary conditions at the fixed repulsion parameter $a_{AB} = 50$ for $N_A = N_B = 2, 5, 10$ and at the fixed block length $N_A = N_B = 5$ for $a_{AB} = 30, 35, 40, 45, 50, 60$, and 80. In all the cases, an equilibrium lamellar microstructure was formed within 2×10^4 units of dimensionless time. Its structural characteristics were averaged over 100 configurations selected by the time step $\Delta t = 40$.

Let us introduce an order parameter

$$\theta_X = \langle \phi_{X,r_c} \rangle - \phi_X^0, \phi_X = \rho_X / \rho_0, \quad X = A, B \quad (\text{A.1})$$

where ϕ_{X,r_c} is the volume fraction of X-particles within the cutoff distance r_c ($r_c = 1$ was taken) from a selected particle of type X, ϕ_X^0 is the mean fraction of X-particles in the system. Brackets denote averaging over the surrounding of all X-particles.

Evolution of the order parameter θ_A from a disordered initial state to the equilibrium is shown in Figure A1.

The behavior of different curves in Figure A1 cannot be described with a universal dependence. Therefore, we postulated

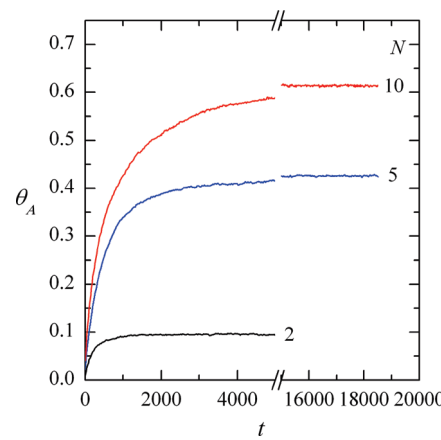


Figure A1. Time dependence of the order parameter θ_A for AB diblock copolymer melts at different block lengths N . The repulsion parameter $a_{AB} = 50$.

Table A1. Ordering in AB Diblock Copolymer Melts and Influence of the Block Length N

N	c_∞	d	$t_{1/2}$
2	1.188	1.5838 ± 0.0007	157.3
5	0.845	2.8158 ± 0.0044	380.3
10	0.630	4.1944 ± 0.0011	470.1

Table A2. Ordering in AB Diblock Copolymer Melts and Influence of the Repulsion Parameter a_{AB}

a_{AB}	χ_{AB}	c_∞	d
30	1.53	0.35567	1.1856 ± 0.0007
35	3.06	0.60804	2.0268 ± 0.0063
40	4.59	0.75360	2.5120 ± 0.0081
45	6.12	0.80431	2.6810 ± 0.0092
50	7.65	0.84475	2.8158 ± 0.0044
60	10.71	0.89741	2.9914 ± 0.0060
80	16.83	0.98803	3.2934 ± 0.0101

that the characteristic time of a microstructure formation, $t_{1/2}$, satisfies the condition

$$\theta_A(t_{1/2}) = \frac{\theta_A(0) + \lim_{t \rightarrow \infty} \theta_A(t)}{2} \quad (\text{A.2})$$

Since $\theta_A \approx 0$ in the initial state, $t_{1/2}$ is the time that is necessary to attain half of the order parameter value in the equilibrium state.

Simulation results for $t_{1/2}$, the equilibrium number density of copolymer molecules (per unit area of lamellar surface) c_∞ , and the domain width d are summarized in Tables A1 and A2.

An accurate determination of c_∞ and d was possible with implementing the procedure for calculating the area of a polymer/polymer interface known as the “marching cubes” algorithm,⁵⁰ which is described in Appendix B.

Appendix B. Calculation of the Interfacial Area in a Polymer Blend

Here we briefly describe the procedure of calculating the area of a polymer/polymer interface. Let us introduce an auxiliary potential generated by particles, which may be an arbitrary function decreasing with distance and having different signs in A and B phases. In this work, the potential created at point \mathbf{r} by i -th particle situated at point \mathbf{r}_i is taken in a simple spring-like form:

$$\omega(\mathbf{r}, \mathbf{r}_i) = \begin{cases} \epsilon(r_c - |\mathbf{r} - \mathbf{r}_i|)^2, & r < r_c \\ 0, & r \geq r_c \end{cases} \quad (\text{B.1})$$

where ϵ_i equals 1 for particle A and -1 for particle B. It is easy to check that the net potential

$$\Omega(\mathbf{r}) = \sum_i \omega(\mathbf{r}, \mathbf{r}_i) \quad (\text{B.2})$$

has different signs within the phases A and B.

The A/B interface is identified with a surface, where $\Omega(\mathbf{r})$ takes zero value. Its area can be calculated using the “marching cubes” cell-based triangulation scheme.⁵⁰ The simulation box is covered with a simple cubic lattice. Triangulation is performed separately for each lattice cell crossed by the interface. The values of $\Omega(\mathbf{r})$ are calculated at all lattice vertices and edges connecting the vertices with different sign of $\Omega(\mathbf{r})$ are detected. Assuming a linear dependence of the net potential along edges, one finds edge points, where $\Omega(\mathbf{r}) \approx 0$. These points belong to the interface and in each cell can be considered as vertices of a polygon. In this work, such polygons are determined “on the fly” in contrast to the original algorithm,⁵⁰ where a set of templates is used. If a polygon has more than three vertices, an extra point is added as the “center of masses” of those vertices and a perpendicular to the interface is dropped from it. The intersection point is used as a common vertex for dividing the polygon into triangles.

The “marching cubes” algorithm produces relatively small number of triangles and has high efficiency. Though the generated interface can have small topological defects,⁵⁵ its area converges with decreasing the grid size. Variations in the interface area were less than 1.0% at the grid size of $0.25r_c$, which was used in all calculations.

References and Notes

- (1) *Polymer Blends*; Paul, D. R., Bucknall, C. B., Eds.; Wiley: New York, 2000; 2 Vols.; 1189 pp.
- (2) Xanthos, M.; Dagli, S. S. *Polym. Eng. Sci.* **1991**, *31*, 929.
- (3) Koning, C.; Van Duin, M.; Pagnoulle, C.; Jerome, R. *Prog. Polym. Sci.* **1998**, *23*, 707.
- (4) Litmanovich, A. D.; Platé, N. A.; Kudryavtsev, Y. V. *Prog. Polym. Sci.* **2002**, *27*, 915.
- (5) Macosko, C. W.; Jeon, H. K.; Hoye, T. R. *Prog. Polym. Sci.* **2005**, *30*, 939.
- (6) Adedeji, A.; Lyu, S.; Macosko, C. W. *Macromolecules* **2001**, *34*, 8663.
- (7) Fredrickson, G. H. *Phys. Rev. Lett.* **1996**, *76*, 3440.
- (8) O’Shaughnessy, B.; Sawhney, U. *Phys. Rev. Lett.* **1996**, *76*, 3444.
- (9) Fredrickson, G. H.; Milner, S. T. *Macromolecules* **1996**, *29*, 7386.
- (10) O’Shaughnessy, B.; Vaylonis, D. *Europhys. Lett.* **1999**, *45*, 638.
- (11) O’Shaughnessy, B.; Vaylonis, D. *Eur. Phys. J. E* **2000**, *1*, 159.
- (12) Yeung, Ch.; Herrmann, K. A. *Macromolecules* **2003**, *36*, 229.
- (13) Müller, M. *Macromolecules* **1997**, *30*, 6353.
- (14) Yang, Y.; Char, K. *Macromol. Theory Simul.* **2001**, *10*, 565.
- (15) John, A.; Nagel, J.; Heinrich, G. *Macromol. Theory Simul.* **2007**, *16*, 430.
- (16) Cheng, M. H.; Balazs, A. C.; Yeung, Ch.; Ginzburg, V. V. *J. Chem. Phys.* **2003**, *118*, 9044.
- (17) Oyama, H. T.; Inoue, T. *Macromolecules* **2001**, *34*, 3331.
- (18) Yin, Z.; Koulic, C.; Pagnoulle, C.; Jérôme, R. *Langmuir* **2003**, *19*, 453.
- (19) Harton, S. E.; Stevie, F. A.; Spontak, R. J.; Koga, T.; Rafailovich, M. H.; Sokolov, J. C.; Ade, H. *Polymer* **2005**, *46*, 10173.
- (20) Kim, B. J.; Kang, H.; Char, K.; Katssov, K.; Fredrickson, G. H.; Kramer, E. J. *Macromolecules* **2005**, *38*, 6106.
- (21) Kim, B. J.; Fredrickson, G. H.; Kramer, E. J. *Macromolecules* **2007**, *40*, 3686.
- (22) Chi, C.; Hu, Y. T.; Lips, A. *Macromolecules* **2007**, *40*, 6665.
- (23) Orr, C. A.; Cernohous, J. J.; Guegan, P.; Hirao, A.; Jeon, H. K.; Macosko, C. W. *Polymer* **2001**, *42*, 8171.
- (24) Oyama, H. T.; Ougizawa, T.; Inoue, T.; Weber, M.; Tamaru, K. *Macromolecules* **2001**, *34*, 7017.
- (25) Lyu, S. P.; Cernohous, J. J.; Bates, F. S.; Macosko, C. W. *Macromolecules* **1999**, *32*, 106.
- (26) Zhang, J.; Lodge, T. P.; Macosko, C. W. *Macromolecules* **2005**, *38*, 6586.
- (27) Orr, C. A.; Adedeji, A.; Hirao, A.; Bates, F. S.; Macosko, C. W. *Macromolecules* **1997**, *30*, 1243.
- (28) Kim, H. Y.; Jeong, U.; Kim, J. K. *Macromolecules* **2003**, *36*, 1594.
- (29) Bhadane, P. A.; Tsou, A. H.; Cheng, J.; Favis, B. D. *Macromolecules* **2008**, *41*, 7549.
- (30) Hoogerbrugge, P. J.; Koelman, J. M. V. A. *Europhys. Lett.* **1992**, *19*, 155.
- (31) Koelman, J. M. V. A.; Hoogerbrugge, P. J. *Europhys. Lett.* **1993**, *21*, 363.
- (32) Espanol, P.; Warren, P. B. *Europhys. Lett.* **1995**, *30*, 191.
- (33) Groot, R. D.; Warren, P. B. *J. Chem. Phys.* **1997**, *107*, 4423.
- (34) Groot, R. D.; Madden, T. J. *J. Chem. Phys.* **1998**, *108*, 8713.
- (35) Roan, J. R.; Shakhnovich, E. *Phys. Rev. E* **1999**, *59*, 2109.
- (36) Berezkin, A. V.; Khalatur, P. G.; et al., DPDChem version 1.0, http://polymer.physik.uni-ulm.de/~khalatur/exchange/DPD_Chem/index.htm.
- (37) Besold, G.; Vattulainen, I.; Karttunen, M.; Polson, J. M. *Phys. Rev. E* **2000**, *62*, R7611.
- (38) Karttunen, M.; Vattulainen, I.; Besold, G.; Polson, J. M. *J. Chem. Phys.* **2002**, *116*, 3968.
- (39) Semenov, A. N. *Sov. Phys. JETP* **1985**, *61*, 733.
- (40) Nyrkova, I. A.; Khokhlov, A. R.; Doi, M. *Macromolecules* **1993**, *26*, 3601.
- (41) Akkermans, R. L. C.; Toxvaerd, S.; Briels, W. J. *J. Chem. Phys.* **1998**, *109*, 2929.
- (42) Khokhlov, A. R.; Berezkin, A. V.; Khalatur, P. G. *J. Polym. Sci. A., Polym. Chem.* **2004**, *42*, 5339.
- (43) Liu, H.; Qian, H. J.; Zhao, Y.; Lu, Z. Y. *J. Chem. Phys.* **2007**, *127*, 144903.
- (44) Berezkin, A. V.; Solov’ev, M. A.; Khalatur, P. G.; Khokhlov, A. R. *J. Chem. Phys.* **2004**, *121*, 6011.
- (45) Jeon, H. K.; Macosko, C. W.; Moon, B.; Hoye, T. R.; Yin, Z. *Macromolecules* **2004**, *37*, 2563.
- (46) Zhao, W.; Zhao, X.; Rafailovich, M. H.; Sokolov, J.; Composto, R. J.; Smith, S. D.; Russell, T. P.; Dozier, W. D.; Mansfield, T.; Satkowski, M. *Macromolecules* **1993**, *26*, 561.
- (47) Spenley, N. A. *Europhys. Lett.* **2000**, *49*, 534.
- (48) Guégan, P.; Macosko, C. W.; Ishizone, T.; Hirao, A.; Nakahama, S. *Macromolecules* **1994**, *27*, 4993.
- (49) Lowe, C. P. *Europhys. Lett.* **1999**, *47*, 145.
- (50) Lorensen, W. E.; Cline, H. E. *Comput. Graphics* **1987**, *21*, 163.
- (51) Walton, J. E. R. B.; Tildesley, D. J.; Rowlinson, J. S. *Mol. Phys.* **1983**, *48*, 1357.
- (52) Nijmeijer, M. J. E.; Bakker, A. E.; Bruin, C.; Sikkenk, J. H. *J. Chem. Phys.* **1988**, *89*, 3789.
- (53) Macosko, C. W.; Guegan, P.; Khandpur, A. K.; Nakayama, A.; Marechal, P.; Inoue, T. *Macromolecules* **1996**, *29*, 5590.
- (54) Snodergaard, K.; Lyngaae-Jorgenson, J. *Polymer* **1996**, *37*, 509.
- (55) Düurst, M. J. *Comput. Graphics* **1988**, *22*, 72.